Appl. Phys. A (2017) 123:732
DOI 10.1007/s00339-017-1360-0

Applied Physics A
Materials Science & Processing

Room temperature magneto-electric coupling in La–Zn doped $Ba_{1-x}La_xFe_{12-x}Zn_xO_{19}$ ($x = 0.0$–0.4) hexaferrite

Pawan Kumar[1] · **Anurag Gaur**[1]

Received: 27 June 2017 / Accepted: 27 October 2017 / Published online: 3 November 2017
© Springer-Verlag GmbH Germany 2017

Abstract Barium hexaferrite powder samples with substitution of La^{+3} at Ba^{+2} and Zn^{+2} at Fe^{+3} site, according to the series formula $Ba_{1-x}La_xFe_{12-x}Zn_xO_{19}$ ($x = 0.0$, 0.1, 0.2, 0.3, 0.4) have been prepared by the co-precipitation method. These samples were characterized by X-ray diffractometer (XRD), scanning electron microscopy, Polarization versus electric field loop tracer and vibrating sample magnetometer techniques. XRD patterns and Rietveld refinement indicate the single-phase formation of the magneto-plumbite barium hexaferrite for all the samples. Significant changes in dielectric properties are obtained by the different doping concentration of La and Zn. Ferroelectric loop for all the samples shows the lossy ferroelectric behaviour. Large spontaneous polarization is observed for $x = 0.2$ sample at room temperature. With increasing La and Zn doping content, the value of saturation magnetization and retentivity increases, and reaches a maximum value of 40.0 emu/gm and 24.0 emu/gm, respectively, for $x = 0.2$ sample and then decreases. To confirm the magneto-electric coupling, the second-order magneto-electric coupling coefficient β is measured through the dynamic method with the maximum value of $\sim 1.69 \times 10^{-6}$ mV/cm.Oe^2 for $x = 0.2$ sample at room temperature. The observations of room temperature magneto-electric coupling in these samples are useful for evolution of new multifunctional devices.

✉ Anurag Gaur
anuragdph@gmail.com

[1] Department of Physics, National Institute of Technology, Kurukshetra 136119, India

1 Introduction

Multiferroic materials have been receiving huge attention from the previous few years, in which both ferroelectric and magnetic properties find together in single-phase materials. These materials display the magneto-electric effect, by the interaction between ferroelectric and ferromagnetic ingredient, in which the magnetization is induced by changing the electric field or electrical polarization induced by changing the magnetic field. However, materials which have both properties ferroelectricity and ferromagnetism simultaneously are rare [1, 2] and most of them show weak magneto-electric effect. The magnetic properties of the hexagonal ferrite are intrinsically linked with their crystalline structure. M-type hexagonal ferrite, $BaFe_{12}O_{19}$, is an extensively studied permanent magnetic material among others because of its high saturation magnetization, good chemical stability, high coercivity and large magneto-crystalline anisotropy [3], and room temperature ferromagnetic and insulating properties. One unit cell of M-type hexaferrite made by two molecular units contained four S, R, S*and R* blocks. The S and S* blocks have oxygen and iron atoms in spinal forms, and R and R* blocks have barium, oxygen and iron atoms in the hexagonally forms. The S and S* block are rotated 180° about the c-axis and separate by the R block. These four blocks in a unit cell are alternately extended in the form of hexagonally and cubically packed layers [4]. Barium hexaferrite has a hexagonal crystal structure with space group $P6_3/mmc$ in which the iron atoms occupy at five different crystallography sites with a uniaxial magnetic anisotropy [4]. Slama et al. [5] show that the electronic state and the occupying dopants ion at different crystallography site in place of an iron site has enormous impact on the magnetic properties of the barium hexaferrite. Slight change of the ferroelectrics properties has been observed in lead-doped

barium hexaferrite [6]. Wang and Xiang investigated a strong indication of exhibiting frustrated antiferroelectricity due to the interaction between the local dipoles caused by the displacements of the trigonal bipyramidal (TBP) Fe^{+3} ions by considering the five different dipole arrangements in M-type $BaFe_{12}O_{19}$ hexaferrite [7]. Recently, Tan and Li obtained both ferroelectric and ferromagnetic properties in a single-phase $PbFe_{12}O_{19}$ hexaferrite [8]. Kostishyn et al. observed magnetic and ferroelectric properties in hexagonal $SrFe_{12}O_{19}$ and $BaFe_{12}O_{19}$ ferrites, sintered these ferrites in the presence of oxygen using boron oxide [9]. Kimura Tsuyoshi and Nakamura Hiroyuki report a low-field magneto-electric effect in Z-type hexaferrite ($Sr_3Co_2Fe_{24}O_{41}$) at room temperature [10].

The intrinsic magnetic and ferroelectric strength of single-phase M-type ferrite materials can be improved by changing the synthesis of environment or by partial replacement of divalent metal or Fe ions, or both. Xie et al. [11] and Suriya Ounnunkad [12] reported that the substitution of La^{+3} ions increases the saturation magnetization of the M-type hexaferrite powder. However, the extensive ferroelectric aspect of the doped $BaFe_{12}O_{19}$ compound has not been reported yet.

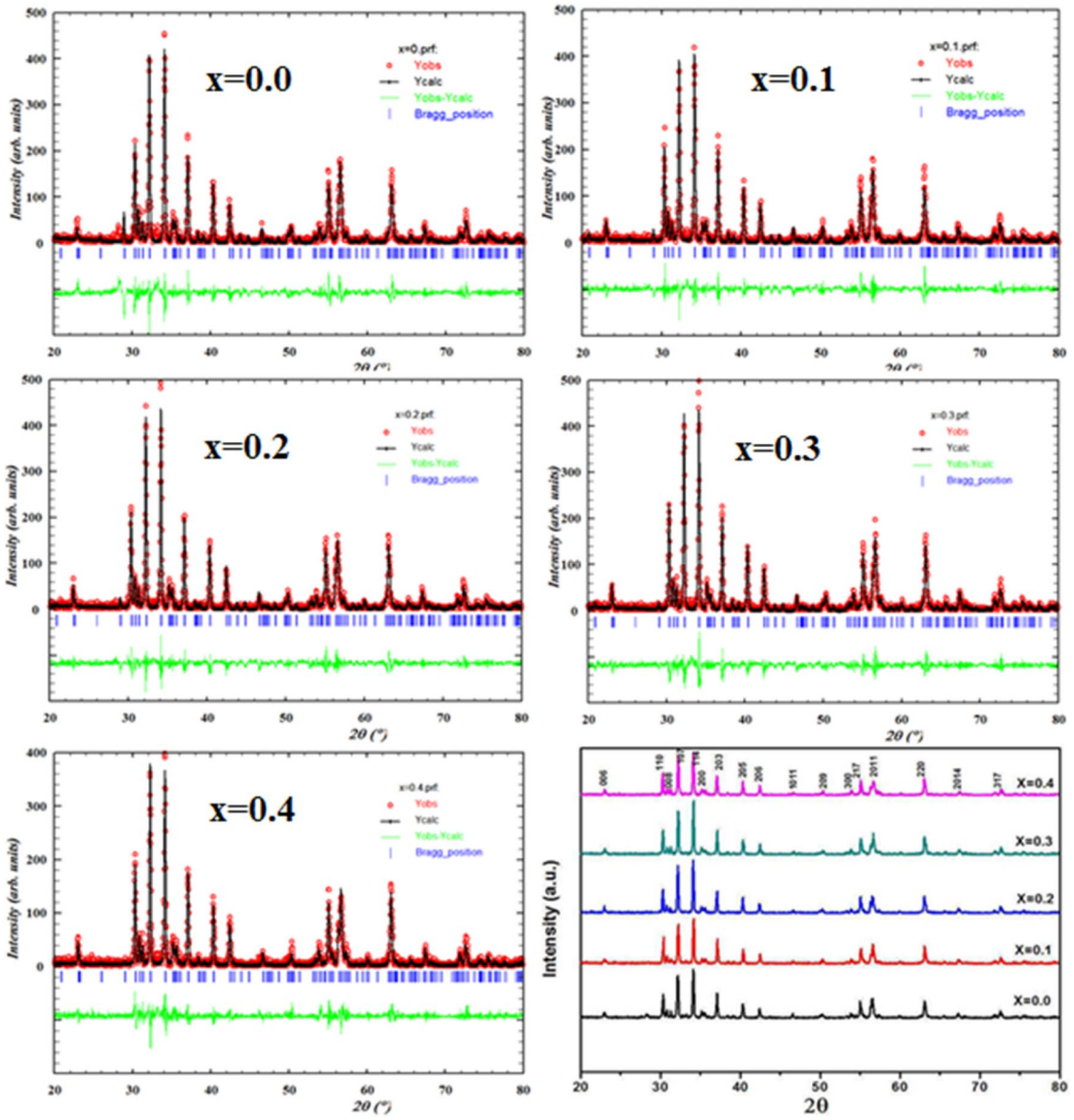

Fig. 1 Rietveld refinement and X-ray diffraction patterns of $Ba_{1-x}La_xFe_{12-x}Zn_xO_{19}$

Table 1 Variations of average crystallite size and lattice parameters of $Ba_{1-x}La_xFe_{12-x}Zn_xO_{19}$

Doping content (x)	Crystallize size (nm)	Lattice parameters (Å)	
		a	c
0	~47	5.887	23.190
0.1	~45	5.879	23.175
0.2	~44	5.864	23.164
0.3	~43	5.863	23.157
0.4	~42	5.862	23.135

In view of the above, we have synthesized La–Zn-substituted $BaFe_{12}O_{19}$ by chemical co-precipitation method and study its magnetic, ferroelectric and magneto-electric properties. It is observed that substitution of La at Ba site and Zn at Fe site strongly affects the magneto-electric properties of this compound and enhances the magneto-electric coupling at room temperature.

2 Experimental procedure

All the samples of Ba-hexaferrites $Ba_{1-x}La_xFe_{12-x}Zn_xO_{19}$ ($x = 0.0, 0.1, 0.2, 0.3, 0.4$) were synthesized by co-precipitation and citrate combustion process. High-purity reagent grade raw materials without further purification were used for preparing the samples.

These samples have been prepared according to the following chemical equation:

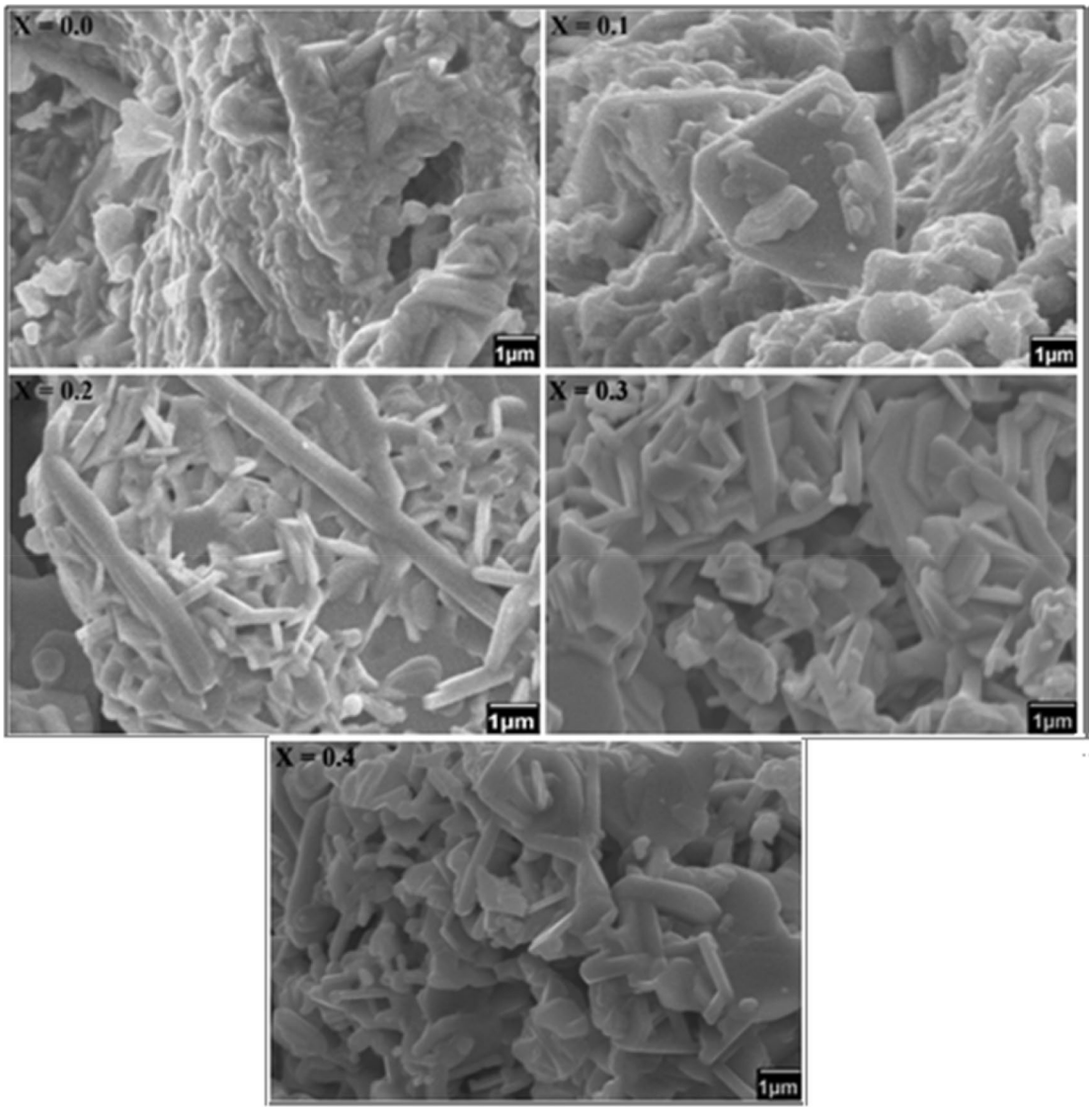

Fig. 2 SEM photographs of $Ba_{1-x}La_xFe_{12-x}Zn_xO_{19}$

$$(1-x)\mathrm{Ba(CH_3COO)_2} + x\mathrm{La(NO_3)_3}\cdot 6\mathrm{H_2O} + (12-\mathrm{X})\mathrm{Fe(NO_3)_3}\cdot 9\mathrm{H_2O} + x\mathrm{Zn(NO_3)_2}\cdot 6\mathrm{H_2O} \xrightarrow{\text{Citric acid /ammonia solution}} \mathrm{Ba_{(1-x)}La_xFe_{(12-x)}Zn_xO_{19}}$$

According to $Ba_{1-x}La_xFe_{12-x}Zn_xO_{19}$ stoichiometric amounts of Barium acetate ($Ba(CH_3COO)_2$), Lanthanum nitrate hexa-hydrate ($La(NO_3)_3{\cdot}6H_2O$), ferric nitrate Nona-hydrate ($Fe(NO_3)_3{\cdot}9H_2O$) and Zinc nitrate hexa-hydrate ($Zn(NO_3)_2{\cdot}6H_2O$) and citric acid were dissolved in deionized water. The precipitation reaction occurred after adding drop by drop ammonia solution in mixed metal solution and during this process, the pH value of the solution was adjusted to pH-12. For these sample preparations, citric acid and the metal ions have been used in 1:1 ratio. The transparent solutions were heated at 80 °C with regular stirring. After heating, these transparent solutions were converted into the gels. Further, the brown ferrite powder was obtained by the gel precursors combusted at 250 °C. The brown ferrite powders were ground and calcined at 1200 °C for 2 h. After that, pellets were formed using Hydraulic pressure machine at 5 MPa/cm^2 and finally, these pellets were annealed at 200 °C for 2 h in a furnace. Crystal structure for all the prepared samples have been determined using a powder X-ray Diffractometer (Rigaku Mini Flex 200, $\lambda = 1.54$ A°) with CuKα radiation. Morphology of all samples was observed through the Scanning Electron Microscopy (SEM). Magnetic hysteresis traces were recorded by the vibrating sample magnetometer (Lakeshore VSM 7304) and ferroelectric loops were recorded by the P–E loop tracer. The dielectric measurement from 20 Hz to 1 MHz frequency range was carried out by LCR meter (Wayne Kerr 4100 series) at room temperature. For the magneto-electric properties, we have used homemade experimental setup.

3 Results and discussion

The powder X-ray diffraction patterns and Rietveld refinement for all the prepared $Ba_{1-x}La_xFe_{12-x}Zn_xO_{19}$ samples (where $x = 0$, 0.1, 0.2, 0.3, 0.4) are shown in Fig. 1. The result revealed that all the ferrite samples have pure phase of M-type barium ferrite (JCPDS card no. 27-1029) without any extra reflection. It is also confirmed that all samples are concoctive by magneto-plumbite crystal structure. In addition, it indicates that the La^{3+} and Zn^{2+} have entered in to the lattice of the $Ba_{1-x}La_xFe_{12-x}Zn_xO_{19}$ as no separate peaks corresponding to these precursors are observed. Table 1 lists the lattice parameters and crystallite size of La and Zn-substituted barium ferrite, calculated using XRD data. The crystallite size and the lattice parameter decrease as the doping content increases due to less ionic radius of La^{3+} ion (0.106 nm) and Ba^{2+} (0.135 nm) ion.

Figure 2 shows the SEM pictures of $Ba_{1-x}La_xFe_{12-x}Zn_xO_{19}$ hexaferrite ($x = 0.0$, 0.1, 0.2, 0.3, 0.4) samples. The SEM image for $x = 0.0$ and 0.1 sample show the strong agglomeration of particles. However, sharp and well-defined edges of platelets like hexagonal structures are observed for $x = 0.2$, 0.3 and 0.4 samples. It is also found that the size and shape of platelets are not varying uniformly as per increase in La and Zn concentration.

Figures 3 and 4 show the variation of dielectric constant ($\acute{\varepsilon}$) and dielectric loss (tanδ) for all the samples between the frequency range 20 Hz and 1MHz. These figures revealed that the values of dielectric constant ($\acute{\varepsilon}$) and dielectric loss (tanδ) are decreasing with increasing frequency for all the samples. It can be explained on the basis of Maxwell–Wagner theory, which is generally used to describe the dielectric properties of solid material. According to Maxwell–Wagner, the grain and the grain boundary acts as a resistor and thin insulating layer in a bulk material. The charge conduction phenomena in ferrite are generated due the exchange of electron between Fe^{+2} and Fe^{+3} present at octahedral sites. As the frequency increases with external applied electric field, the polarization decreases, due to the electron hopping between Fe^{+2} and Fe^{+3} at high frequency, which cannot go along with the alternating field. The value of dielectric constant increases with increasing doping content of La–Zn. The samples with larger zinc and lanthanum doping content have larger quantity of Fe^{+2} ions because of the possibility that zinc content evaporation would be larger in these samples. Similar results were obtain by Dube et al. [13] and the substitution of La^{+3} on Ba^{+2} site which creates the charge imbalance in ferrite structure; therefore to maintain charge symmetry, some of the Fe^{+3} ions at the octahedron sites convert into Fe^{+2} ions at the tetrahedron sites. Further Fe^{+2} ions are the borderline acids and easily polarized, so the ferrite with higher concentration of La and Zn would have high

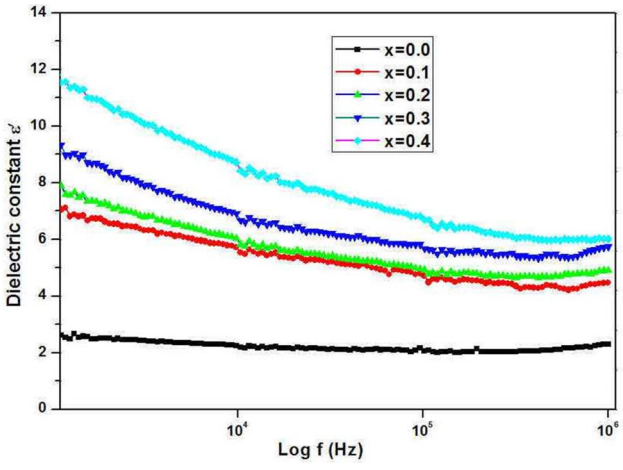

Fig. 3 Dielectric constant versus frequency curve of $Ba_{1-x}La_xFe_{12-x}Zn_xO_{19}$ at room temperature

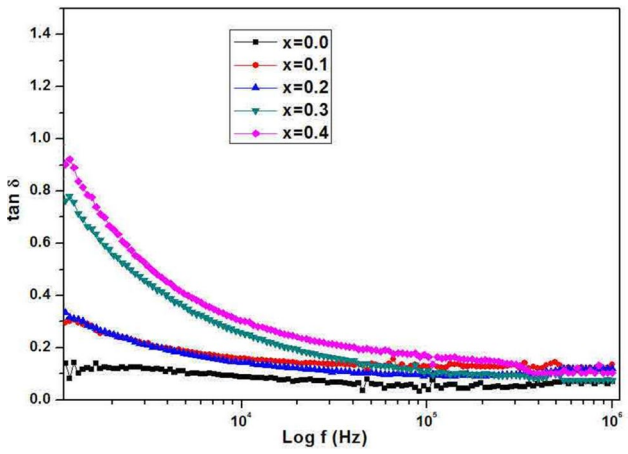

Fig. 4 Dielectric loss (tanδ) versus frequency curve of $Ba_{1-x}La_xFe_{12-x}Zn_xO_{19}$ at room temperature

dielectric constant. The electron exchange between Fe^{+3} and Fe^{+2} ions results in higher dielectric loss, and the excess Fe^{+2} reinforces the interfacial polarization for substituted samples. Moreover, the extra intrinsic electric moment is created in samples due the distinct radius of La^{+3} from the other cations. Thus, values of dielectric constant and dielectric loss get larger with La^{+3} and Zn^{+2} substitutions in place of Ba^{+2} and Fe^{+3} in the M-type hexaferrite.

Polarization versus electric field (P–E) loops for preparing samples $Ba_{1-x}La_xFe_{12-x}Zn_xO_{19}$ ($x=0.0$–0.4) are shown in Fig. 5a at room temperature. The hysteresis loops show the lossy ferroelectric behaviour for all the samples. It is observed through PE loops that the values of remanent polarization (Pr), maximum polarization (Ps) and the coercive electric field (Ec) first increase with increase the doping content of La–Zn up to $x=0.2$ and then decrease as shown in Fig. 5b. The maximum value of Pr, Ps and Ec are obtained 3.52, 11.11 μC/cm^2 and 1.10 kV/cm, respectively, for the $x=0.2$ sample. The increment in value of Pr, Ps and Ec can be described on the basis

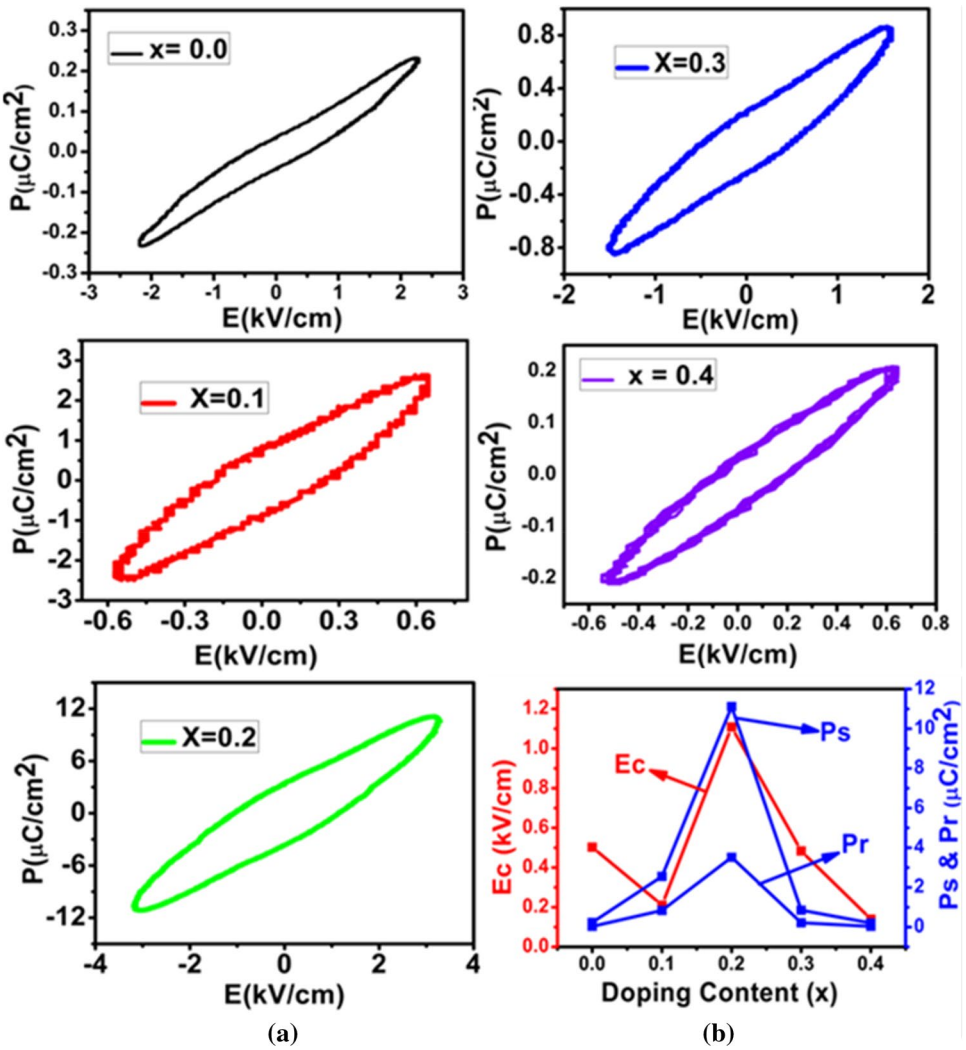

Fig. 5 **a** Polarization versus electric field (P–E) hysteresis loops of $Ba_{1-x}La_xFe_{12-x}Zn_xO_{19}$ at room temperature. **b** Remanent polarization (Pr), Maximum polarization (Ps) and the Coercivity (Ec) with doping content (x)

of charge ordering in magnetic materials, which is observed in the systems with ions that formally have a mixed valence [14]. A chain of alternative charge magnetic ions breaks inversion symmetry on the magnetic site which induced electric polarization through exchange striction interaction. M-type barium ferrite structure formed by close packing of cubic and hexagonal-stacked layer of oxygen and barium ions with Fe ions at five different interstitial sites. Iron ions have formed octahedral at 12k, $4f_2$, and 2a site, tetrahedral at $4f_1$ site and trigonalbipyramidal at (2b) site. According to the Mössbauer spectroscopy results reported [15]; Zn^{+2} ions are occupied at the spin-down $4f_1$ site in place of Fe^{+3} ions. Here the off-centre polarization developed along the $4f_1$–2a–$4f_1$ zigzag chain [16], due to the change in spin configuration associated with the local spin reversal at the 2a sites along this zigzag chain as shown in Fig. 6. Further, increase in the doping content ($x > 0.2$) results in the decrease of value of Pr, Ps and Ec due to decrease in off-centre polarization developed along zigzag chain.

Figure 7 shows M–H hysteresis loop for La–Zn doped $Ba_{1-x}La_xFe_{12-x}Zn_xO_{19}$ samples with $x = 0.0$, 0.1, 0.2, 0.3, 0.4 recorded at room temperature. The influence of La–Zn doping content on the saturation magnetization (M_S) and retentivity (Mr) for these samples are shown in the inset of Fig. 7. The value of M_S and Mr first increases gradually with doping content and reaches to the maximum value of 40.0 and 24.0 emu/g for $x = 0.2$ sample and then decreases for the samples above $x = 0.2$, respectively. The similar trend of results was observed by Liu et al. [17] for La–Mn- and La–Co-substituted barium hexaferrites. The change in retentivity and saturation magnetization with the substituted-ion element of La–Zn can be described by the super exchange interaction between the magnetic ions at different site. It is well known that the magnetic moment in ferrite has been enormously generated by the Fe atoms. In M-type hexaferrite iron, atoms have a parallel spin to each other at 12k, 2a, and 2b sites and opposite to those iron atoms exist at $4f_1$, $4f_2$ sites. The increments in saturation magnetization value due to the higher hyperfine fields at bipyramidal and octahedral (12k) sites by enhancement in the Fe–O–Fe super exchange interaction increase overall magnetization. Further, the decrement in saturation magnetization (M_S) value could be the cause of substitution of F^{+3} by the larger Zn^{+2} which decreases exchange interaction, and also the Fe–O–Fe super exchange interaction is declined by changing the Fe^{+3} ion state in to Fe^{+2} ion state at 2a site by substitution of the La^{+3} at Ba^{+2} site. Furthermore, it has been observed that coercivity decreases up to $x = 0.3$ sample and then increases for $x = 0.4$ sample. It is explained by the reduction of the magneto-crystalline anisotropy in doped samples due to the substitution of Zn ions at Fe site and also by the difference in particle size and morphology of the sample, which changes the magnetic properties. The coercivity sharply increases

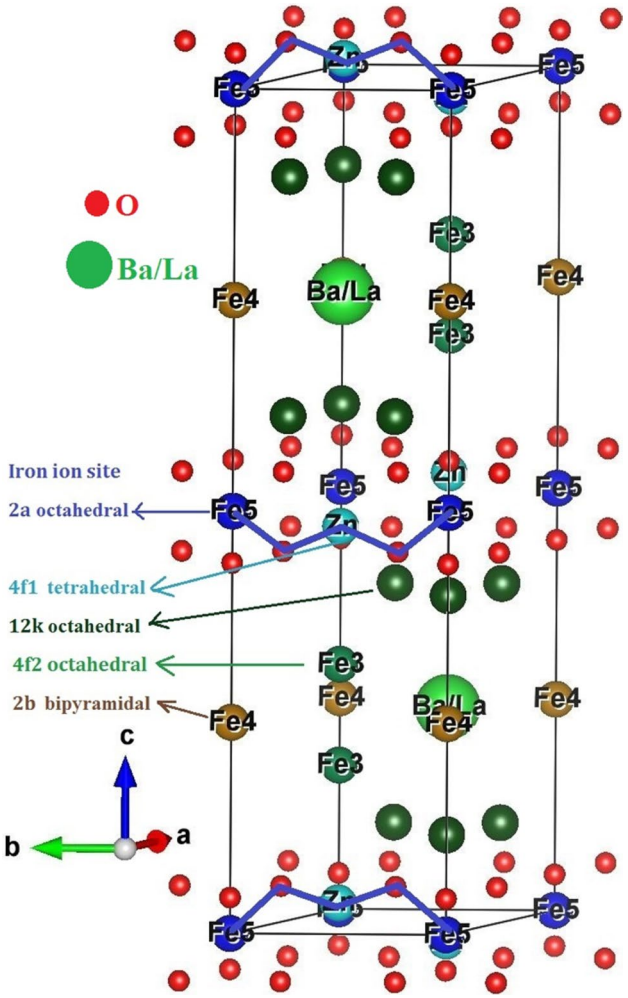

Fig. 6 Crystal structure of $BaFe_{12}O_{19}$ in which Zn occupies the iron ions site at $4f_1$ tetrahedral, blue circles shows the iron at 2a octahedral site with alternative chain $4f_1$–2a–$4f_1$ in which the red circles shows the oxygen atoms

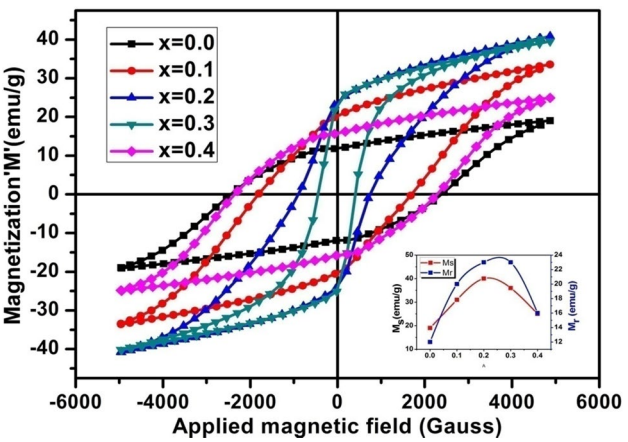

Fig. 7 Magnetisation versus magnetic field (M–H) hysteresis loop of $Ba_{1-x}La_xFe_{12-x}Zn_xO_{19}$ at room temperature. Inset shows the variation in saturation magnetization (M_S) and retentivity (Mr) with La–Zn doping content

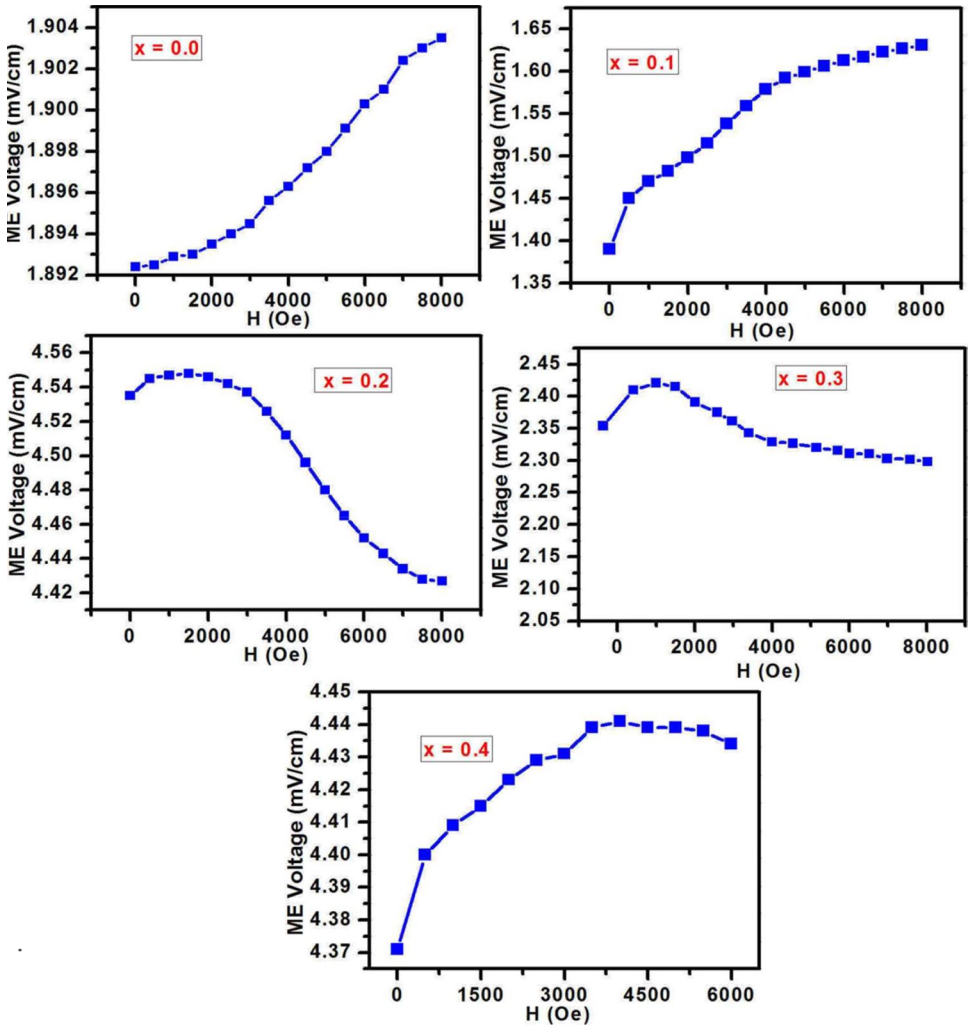

Fig. 8 Variation in magneto-electric voltage with dc magnetic field for La–Zn substitution for $Ba_{1-x}La_xFe_{12-x}Zn_xO_{19}$ samples

for the sample $x = 0.4$ because of the maximum magneto-crystalline anisotropy. Enhancement in magneto-crystalline anisotropy due to the higher amount of substitute La ions enter into the lattice, and previous study shows [18] that the coercivity of the rare earth element-doped barium hexaferrite increase by La content.

Magneto-electric behaviour for all the prepare sample has been determined by the dynamic method [19] at room temperature. In dynamic method, magneto-electric coupling voltage measurement was carried out with changing dc magnetic field in the presence of fixed ac field. The magneto-electric effect can be described by the equation: $V \propto (\alpha H + \beta H.H)$, where α and β represent the first- and second-order ME coupling coefficient. When a dc field H_0 is modulated by an ac field h_0, then the total field is represented by $H = H_0 + h_0 \sin(\omega t)$ and the output voltage V_{out} measured with lock-in amplifier at the frequency $\omega(\omega = 2\pi f)$ is given by $V_{out} \propto (\alpha h_0 + \beta h_0.H_0)$.

We can find the linear term α by keeping field $(H_0 = 0)$ by varying the ac field and the second-order term β is evaluated by increasing the dc magnetic field at a constant value of ac field. The induced magneto-electric voltage with varying dc bias magnetic field at a constant value of ac magnetic field of 5 Oe at 997 Hz frequency for all doped $Ba_{1-x}La_xFe_{12-x}Zn_xO_{19}$ samples are shown in Fig. 8. The average value of ME second-order coupling coefficient (β) calculated from the Fig. 8 for all samples of $Ba_{1-x}La_xFe_{12-x}Zn_x0_{19}$ ($x = 0.0$, 0.1, 0.2, 0.3, 0.4) are $\sim 7.05 \times 10^{-7}$, $\sim 5.48 \times 10^{-7}$, $\sim 1.69 \times 10^{-6}$, $\sim 9.01 \times 10^{-7}$ and $\sim 1.62 \times 10^{-6}$ mV/cm.Oe^2, respectively. Here, we have find maximum coupling coefficient (β) for $x = 0.2$ sample. The magneto-electric coupling in these samples is explained by the La–Zn substitute structure of bariumhexaferrite as shown in Fig. 9. As already discussed above, M-type hexaferrite structure contained 24 iron atoms in a unit cell which are occupied at five different sites namely: octahedral (12k, 2a and $4f_2$), tetrahedral (4f1) and trigonal bipyramidal (2b) sites [4]. The directions of spin polarization are represented by the arrows on Fe ions. Wartewig et al. reported in 1999 [20] that Zn occupy the iron ions at $4f_1$ tetrahedral site and as a

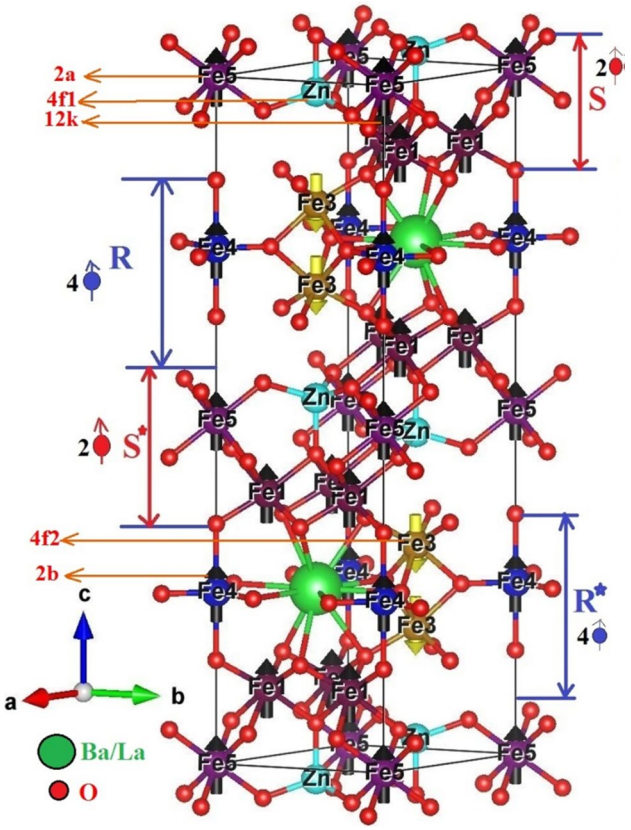

Fig. 9 Crystal structure of $BaFe_{12}O_{19}$ in which Zn occupy the iron ions site at $4f_1$ tetrahedral, and spin moment of iron atom in R block at 12k, 2b and $4f_2$ site have their 4 spin up and S block at 12k, $4f_1$ and 2a site have their 2 spin up which make the alternate S and R block of large and small spin moment

result the total spin moment of iron atom in R block 12k, 2b and $4f_2$ site have their four spin up and S block at 12k, $4f_1$ and 2a site have their two spin up which make the alternate block of large and small spin moment, as shown in Fig. 9. Further, it may be possible that after applying the magnetic field, the longitudinal conical spin structure convert into the transverse conical structure as in $BaFe_{12-x-\delta}Sc_xMg_\delta O_{19}$ [21] and the polarization induced by its cycloidal component in terms of inverse Dzyaloshinskii-Moriya (DM) mechanism [22]. It is also confirmed through PE loops that the values of remnant polarization (Pr) and maximum polarization (Ps) are maximum for the $x=0.2$ sample.

4 Conclusions

In summary, we have synthesized $Ba_{1-x}La_xFe_{12-x}Zn_xO_{19}$ ($x=0.0., 0.1, 0.2, 0.3, 0.4$) hexaferrite via co-precipitation method and study their structural, dielectric, ferroelectric and magneto-electric properties. It is observed that lattice parameter and crystallite size decrease by La–Zn doping at Ba and Fe site, respectively. SEM analysis shows the formation of hexagonal platelet-like structures. The maximum value of polarization, retentivity (Pr) and the coercivity (Hc) is observed 11.11 μC/cm^2, 3.52 μC/cm^2 and 1.10 kV/cm, respectively for $x=0.2$ sample. Further, maximum value of saturation magnetization (40.0 emu/g) and remenence (24.0 emu/g) is also observed for $x=0.2$ sample. The multifunctional responses of $Ba_{1-x}La_xFe_{12-x}Zn_xO_{19}$ hexaferrite system present ferroelectricity and ferromagnetism coexisting in single system with maximum magneto-electric coupling ($\sim 1.69\times10^{-6}$ mV/cm.Oe^2) at room temperature for $x=0.2$ sample, which is very useful for the evolution of multifunctional devices.

Acknowledgements Author (AG) acknowledges the financial support provided by Council of Scientific and Industrial Research (C.S.I.R.), New Delhi, through Grant No: 03(1370)/16/EMR-II. Author (PK) is thankful to MHRD, Government of India, New Delhi, for providing research fellowship. We are also thankful to chief scientist (R.K Kotnala), NPL Delhi, for providing the magnetic characterization facilities.

References

1. N.A. Hill, J. Phys. Chem. B **104**, 6694 (2000)
2. N. Hur, S. Park, P.A. Sharma, J.S. Ahn, S. Guha, and S.-W. Cheong, Nature **429**, 392 (2004)
3. A. Moitra, S. Kim, S.G. Kim, S.C. Erwin, Y.K. Hong, J. Park, Comput. Condens. Matter **1**, 45 (2014)
4. J. Smit, H.P.J. Wijn Ferrites. (Wiley, New York, 1959)
5. J. Slama, A. Gruskova, M. Papanova, D. Kevicka, R. Dosoudil, V. Jančárik, A. Gonzalez, G. Mendoza, J. Magn. Magn. Mater **272**, 385 (2004)
6. P. Kumar, A. Gaur, R.K. Kotnala, Ceram. Int. **43**, 1180 (2017)
7. P. Wang, H. Xiang, Phys. Rev. X. **4**, 011035 (2014)
8. G.L. tan, Li. Wei., J. Am. Ceram. Soc. **98**, 1812 (2015)
9. V.G. Kostishyn, L.V. Panina, A.V. Timofeev, L.V. Kozhitov, A.N. Kovalev, A.K. Zyuzin, J. Magn. Magn. Mater **400**, 327 (2016)
10. Y. Kitagawa, Y. Hiraoka, T. Honda, T. Ishikura, H. Nakamura, T. Kimura, Nat. Mater. **9**, 797 (2010)
11. Y. Xie, X. Hong, X. Wang, J. Zhao, Y. Gao, Y. Ling, S. Yan, L. Shi, K. Zhang, Synth. Met. **162**, 1643 (2012)
12. S. Ounnunkad, Solid State Commun. **138**, 472 (2006)
13. C.L. Dube, S.C. Kashyap, D.K. Pandya, D.C. Dube, Phys. Status Solidi Appl. Mater. Sci. **206**, 2627 (2009)
14. J. van den Brink, D.I. Khomskii, J. Phys. Condens. Matter. **20**, 434217 (2008)
15. S.W. Lee, S.Y. An, I.B. Shim, C.S. Kim, J. Magn. Magn. Mater. **290**, 231 (2005)
16. E.H. Na, S. Song, Y.M. Koo, H.M. Jang, Acta Mater. **61**, 7705 (2013)
17. Y. Liu, M.G.B. Drew, Y. Liu, J. Wang, M. Zhang, J. Magn. Magn. Mater. **322**, 3342 (2010)
18. S. Ounnunkad, P. Winotai, S. Phanichphant, J. Electroceramics **16**, 357 (2006)
19. M. Mahesh Kumar, A. Srinivas, S.V. Suryanarayana, G.S. Kumar, T. Bhimasankaram, Bull. Mater. Sci. **21**, 251 (1998)
20. P. Wartewig, M.K. Krause, P. Esquinazi, S. Rösler, R. Sonntag, J. Magn. Magn. Mater. **192**, 83 (1999)
21. Y. Tokunaga, Y. Kaneko, D. Okuyama, S. Ishiwata, T. Arima, S. Wakimoto, K. Kakurai, Y. Taguchi, Y. Tokura, Phys. Rev. Lett. **105**, 257201 (2010)
22. H. Katsura, N. Nagaosa, A.V. Balatsky, Phys. Rev. Lett. **95**, 057205 (2005)